

2. J. W. Niemantsverdriet, *Spectroscopy in Catalysis* (Wiley-VCH, Weinheim, Germany, 1993).
 3. H. Topsøe, *Stud. Surf. Sci. Catal.* **130**, 1 (2000).
 4. G. Ertl, H.-J. Freund, *Phys. Today* **52**, 32 (January 1999).
 5. G. A. Somorjai, *Introduction to Surface Chemistry and Catalysis* (Wiley, New York, 1994).
 6. J. V. Lauritsen *et al.*, *J. Catal.* **197**, 1 (2001).
 7. R. A. van Santen, M. Neurock, *Catal. Rev.* **37**, 557 (1995).
 8. P. Raybard, J. Hafner, G. Kresse, S. Kasztelan, H. Toulhoat, *J. Catal.* **190**, 128 (2000).
 9. A. Logadottir *et al.*, *J. Catal.* **197**, 229 (2001).
 10. Z. Paal, G. A. Somorjai, in *Handbook of Heterogeneous Catalysis*, G. Ertl, H. Knözinger, J. Weitkamp, Eds. (VCH, Weinheim, Germany, 1997), vol. 3, pp. 1084–1104.
 11. A. Mittasch, *Adv. Catal.* **2**, 81 (1950).
 12. C. J. H. Jacobsen, *J. Catal.* **200**, 1 (2001).
 13. C. J. H. Jacobsen *et al.*, *J. Mol. Catal. A.* **163**, 19 (2000).
 14. This microscope has a Gatan image filter for EELS

studies and for recording energy-filtered images. The in situ system consists of an environmental cell pumped differentially by a molecular drag pump in the first pumping stage and a turbomolecular pump in the second stage. The design of the environmental cell is adopted from Boyes and Gai at DuPont (26) and constructed by Philips in collaboration with Haldor Topsøe A/S. The in situ cell allows heating and introduction of a controlled, gaseous environment over the sample. A resolution better than 0.16 nm can be achieved at pressures of about 20 mbar and temperatures of about 900°C (dependent on gas pressure and composition).
 15. Z. Kowalczyk *et al.*, *Appl. Catal. A* **184**, 95 (1999).
 16. S. Dahl, J. Sehested, C. J. H. Jacobsen, E. Törnqvist, I. Chorkendorff, *J. Catal.* **192**, 391 (2000).
 17. W. Rarog, Z. Kowalczyk, J. Sentek, D. Skladanowski, J. Zielinski, *Catal. Lett.* **68**, 163 (2000).
 18. G. A. Somorjai, N. Materer, *Top. Catal.* **1**, 215 (1994).
 19. S. Tennison, in *Catalytic Ammonia Synthesis*, J. R. Jennings, Ed. (Plenum, New York, 1991), pp. 303–364.

20. J. J. Mortensen, L. B. Hansen, B. Hammer, J. K. Nørskov, *J. Catal.* **182**, 479 (1999).
 21. S. Dahl *et al.*, *Phys. Rev. Lett.* **83**, 1814 (1999).
 22. S. Dahl, A. Logadottir, C. J. H. Jacobsen, J. K. Nørskov, *Appl. Catal.*, in press.
 23. S. Dahl, E. Törnqvist, I. Chorkendorff, *J. Catal.* **192**, 381 (2000).
 24. L. Forni, D. Molinari, I. Rossetti, N. Pernicone, *Appl. Catal. A* **185**, 269 (1999).
 25. H. Bielawa, O. Hinrichsen, A. Birkner, M. Muhler, *Angew. Chem.* **113**, 1093 (2001).
 26. E. D. Boyes, P. L. Gai, *Ultramicroscopy* **67**, 219 (1997).
 27. We gratefully acknowledge the participation of the CTCL Foundation, Taiwan, in the establishment of the TEM facilities. J.B.W. thanks the Danish Research Academy for supporting a scholarship at the Interdisciplinary Research Center for Catalysis (ICAT), Technical University of Denmark.

16 July 2001; accepted 12 October 2001

Seismic Evidence of an Extended Magmatic Sill Under Mt. Vesuvius

Emmanuel Auger,¹ Paolo Gasparini,¹ Jean Virieux,² Aldo Zollo¹

Mt. Vesuvius is a small volcano associated with an elevated risk. Seismic data were used to better define its magmatic system. We found evidence of an extended (at least 400 square kilometers) low-velocity layer at about 8-kilometer depth. The inferred S-wave (~0.6 to 1.0 kilometer per second) and P-wave velocities (~2.0 kilometer per second) as well as other evidence indicate an extended sill with magma interspersed in a solid matrix.

Mt. Vesuvius is a strato volcano near a densely populated area. It is located in a tectonic graben formed in the Plio-Pleistocene, and it is only a few km southeast of Fields, the active volcano on which the city of Napoli has been built (Fig. 1). It experienced at least three violent explosive eruptions in historical times (79, 472, and 1631 A.D.). More frequent, less explosive eruptions have occurred from 1631 to 1944 (1). Mt. Vesuvius is presently in a quiescent state, characterized by low-temperature fumaroles (less than 100°C) and moderate seismic activity (about 100 earthquakes per year with magnitudes between 0.5 and 3.6), and it is difficult to predict when it may erupt explosively again. The definition of its structure and of the location and volume of the magma reservoir can be used to help prediction of the scenario of the next eruption and to interpret the pattern of the expected precursory seismic activity and ground deformation. The present volcanic edifice was built in a time span of about 40,000 years, and the total amount of erupted magma can be estimated to be about 50 km³. This would be the minimum volume of the magma

reservoir if it was a closed system. However, Sr, Nd, Pb, and U-Th-Ra data indicate that the magma system underwent a complex, multi-

stage evolution, which is not compatible with a closed magma reservoir (2–7).

Indications of the lithostatic pressure (and hence the depth) under which the Mt. Vesuvius magmas began to crystallize can be obtained from fluid inclusions in phenocrysts and from mineral equilibria in skarn rocks, which are believed to be formed by high-temperature metamorphism of the carbonate wall rocks. Application of these methods to the products of the last eruptions of Mt. Vesuvius (1906 and 1944) suggests the presence of a magma reservoir at less than 3-km depth refilled during the eruptions with magma coming from a deeper (11 to 22 km) reservoir (8, 9). Fluid inclusions in older Mt. Vesuvius explosive and effusive products indicate crystallization depths between 4 and 10 km (10).

A seismic tomography study carried out in

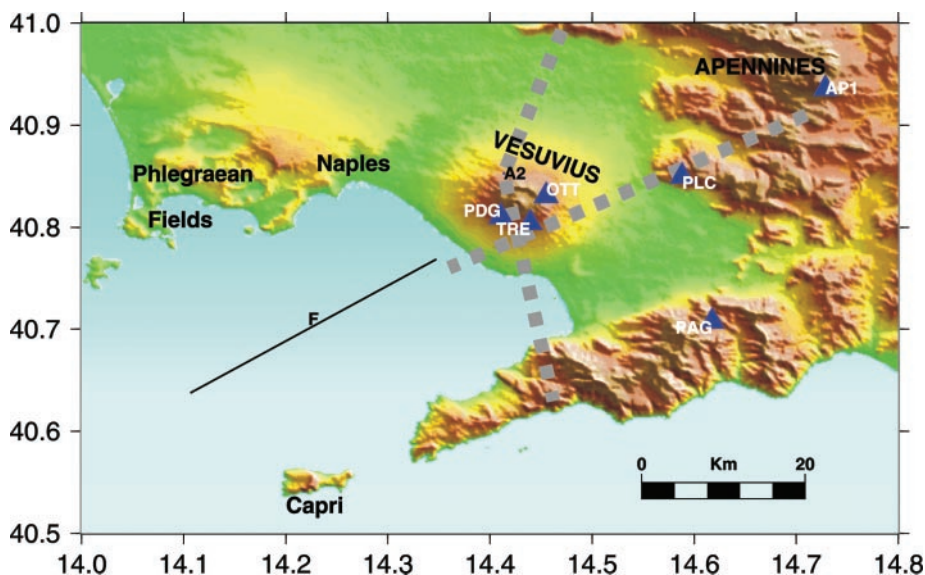


Fig. 1. Sketch map of Mt. Vesuvius area. The black line (F profile of the MAREVES experiment) indicates the profile where the LALA phase is best observed. Blue triangles and three-letter symbols indicate the location of on-land stations of the MAREVES experiment. The gray boxes indicate the points of the mid-crustal interface where the observed LALA phases are generated. They do not correspond to the common midpoint because of P to S conversion.

¹Dipartimento di Scienze Fisiche, Università di Napoli Federico II, Complesso di M. S. Angelo, Via Cinthia, 80124 Napoli, Italy. ²Géosciences Azur, 250 Avenue A. Einstein, 06560 Valbonne, France.

REPORTS

1994 used 84 three-component stations along a single profile to record signals emitted from three underground explosions. One of the most striking results was the observation of a

large-amplitude late arrival phase (LALA), which is stronger in the horizontal components of wave motion, at stations from 10 to 30 km from the source. The relatively low-

frequency content and the dominant horizontal motion indicated that the phase probably originates by a *P* to *S* conversion at the top of a low-velocity layer at mid-crustal depths (about 10 km) (11). The low-velocity layer may be due to a magma reservoir.

Multiprofile seismic experiments were performed in 1996 and 1997. The 1996 experiment consisted of 14 shots recorded by three-components stations along four 30- to 40-km-long profiles intersecting at the top of Mt. Vesuvius. LALA phases were detected in the record of the longest profile at wide angle distances (Fig. 2). The 1997 experiment (MAREVES) used offshore air gun sources and on-land recordings. The experiment consisted of 1800 shots performed by eight synchronous 16-liter air guns from a ship in the Bay of Naples. The seismic signals were recorded by a temporary array of 25 three-component stations deployed in the volcano and in the Apennines as far as 90 km from the coast. Air gun shots were also recorded by the permanent monitoring network of Osservatorio Vesuviano (12).

LALA recordings of shots fired along MAREVES profile F have been processed and depth migrated to get information on the lateral extension, location, and physical properties of the low-velocity layer. Shot profile F and recording stations AP1, PLC, OTT, TRE, and PDG are aligned along a line passing through the volcano and hence fit for two-dimensional (2D) modeling. This line is almost perpendicular to the land profiles along which the LALA phase had been detected (11). Profile F also passes through the zone where the shallow structure has been imaged with the most detail (13). A 2D depth migration technique based on exact ray tracing in heterogeneous media was used to image the velocity structure. Seismic records are back propagated into the medium and stacked along reflected/converted phases' travel time isochrons. An image is obtained where the intensity maxima outline reflecting and/or diffracting bodies (14). This method assumes a 2D background velocity model that was retrieved from first *P*-wave arrival times with the use of travel time tomography at depths shallower than 3 to 4 km and trial and error fitting at higher depth (13, 15). The *S*-wave velocity model was obtained with a V_p/V_s ratio of 1.8, which is the best value obtained by minimizing the arrival times residuals of local earthquakes (16).

An image obtained through the migration of *PS* and *PP* waves at stations AP1, PLC, OTT, TRE, and PDG for the shots of profile F (Fig. 3) shows strong, laterally coherent increase of energy at about 8-km depth. In fact, the stacked energy record exhibits a sharp isolated peak at this depth, indicating the occurrence of an interface with a sharp impedance contrast. Migration of the full waveform synthetics with and

Fig. 2. LALA phase observed on profile A of the 1996 on-land experiment (A) and at station PLC for shots along profile F of the MAREVES experiment (B). The corresponding *PP* phase recorded at station PAG for shots along profile F is shown in (C) (35).

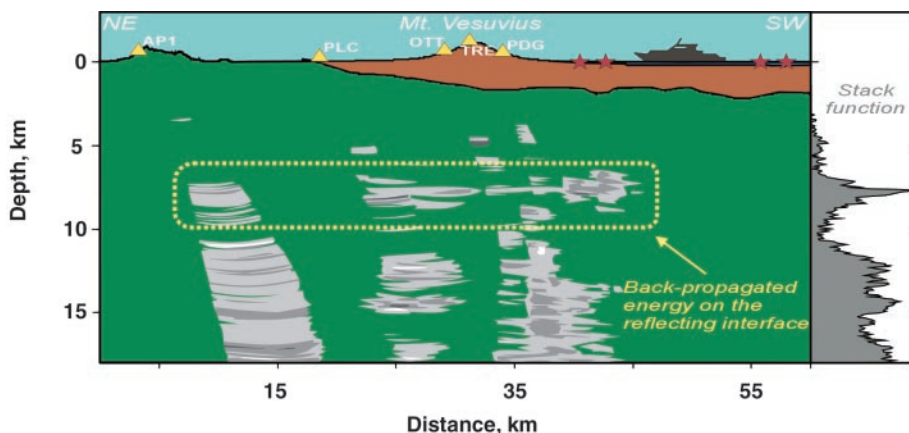
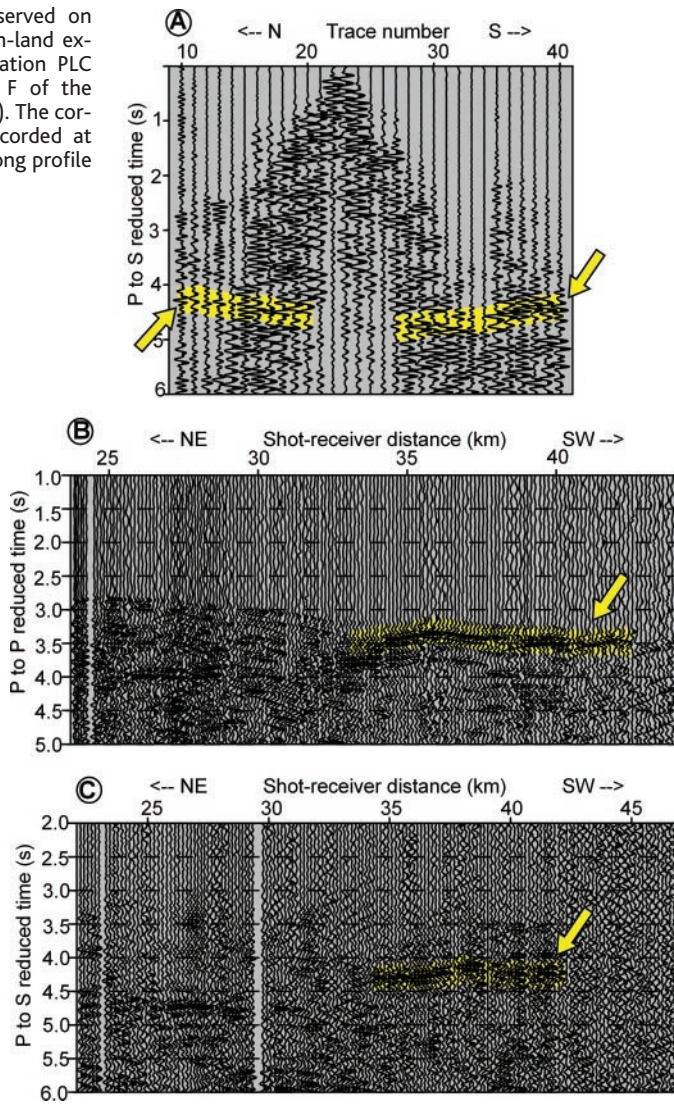


Fig. 3. *PP* and *PS* migrations for shots of profile F and stations PDG, TRE, OTT, PLC, and AP1. A clear increase of energy around 8-km depth is shown on the migrated image. This is still more evident if the energy is summed along horizontal lines, as shown by the plot on the right.

without the interface at 8-km depth (17) showed that the intensity maximum at 8-km depth is not an erroneous back propagation of phases that propagate in the shallow structure. The tests also show that the thickness of the energy peak is related to imperfect focusing of the wave and to the finite duration of the seismic source signal. No clear, laterally coherent focusing of energy occurs between the top of the limestone basement of the volcano (2- to 3-km depth) and the 8-km discontinuity. Synthetic modeling showed that the small isolated energy patches are due to incorrect migration of the first arrivals at some stations located at the slopes of the volcano. Therefore, no evidence exists of any reflectors between the top of the limestone basement and the 8-km discontinuity.

The strong energy concentrations deeper than this discontinuity (Fig. 3) can be associated with multipathing effects in the shallow sedimentary layer and/or multilayer structure below the 8-km interface.

The *PS* phase amplitude variations at different stations were used to estimate the seismic wave velocities below the interface. Amplitude variations are related to the variations of the *P* to *S* reflection coefficient with the incidence angle at the interface, which in turn depends on the velocity contrast. Site effects at shot and receiver locations were accounted for by considering *PS* to first *P* arrival amplitude ratios (18). The *P* to *S* reflection coefficients retrieved from amplitude ratios (Web fig. 1) (19) are compared with theoretical curves computed for different velocities in the underlying medium assuming the same density on both sides of the interface. The observed curve decreases slowly and regularly across a 30° wide angle range, without showing any sharp peak. This pattern constrains the *S*-wave velocity below the interface at less than 1 km/s. It indicates also that *P*-wave velocity decreases below the interface. Additional migration of synthetics computed with different *P*-velocity contrasts suggests that the *P*-wave velocity is around 2 km/s. These values indicate that the 8-km interface is the top of a fluid-containing layer. This is also consistent with results from one-dimensional modeling of magnetotelluric soundings at Mt. Vesuvius, which indicate the occurrence of an electrically conductive layer at about the same depth (20). Mid-crustal low-seismic velocity and high-electrical conductivity layers have often been observed in continental environments. They have been associated with low-viscosity fluids expelled from mid to lower crustal rocks (21). The interpretation has been confirmed by the results of the Kola deep well, Russia, which crosses a mid-crustal seismic discontinuity. It was found to coincide with "the base of a zone of disaggregation related to overpressured fluids" (22, p. 715). In all these cases, the associated *P*-wave velocity decrease is on the order of 20% at most (23–26). This is

not the case of Mt. Vesuvius, where the *S*- and *P*-wave velocities below the 8-km interface are consistent with velocities expected for a magma body hosted in a densely fractured volume of rock (27).

Considering the extension of the reflecting surface along profile F and the orthogonal profile (Fig. 1 and Fig. 3), its area is at least 400 km², and the migrated image suggests that its surface is almost flat (Fig. 3). Low-velocity layers interpreted as magma sills have been identified at 10- to 20-km depth under several volcanoes (27–30). The widespread occurrence of nearly flat magma sills at that depth can be ascribed to neutral buoyancy conditions for magmas uprising from the mantle (31). Under conditions of neutral buoyancy, a slow addition of magma from the mantle to the reservoir will result in the formation of a wide and thin sill in the presence of an extensional tectonic regime (32) similar to that active in the Neapolitan area for the past 2 million years at least.

Our data cannot constrain the thickness of the sill at Mt. Vesuvius. Assuming a thickness of 0.5 to 2.0 km, the minimum overall volume would be 200 to 800 km³, which is consistent with the estimated total volume of magma erupted at Mt. Vesuvius. The extension of this layer would be much larger if it was also the source of the 250 to 300 km³ of magma erupted in the nearby Phlegraean Fields volcanic area in the past 40,000 years.

Long residence times of Mt. Vesuvius magma in a mid-crustal environment are also supported by isotopic data, which indicate contamination from the continental crust. In fact, Sr isotopic ratios (0.7069 to 0.7079) (7), the ³He/⁴He ratio (in the range 2.0 to 2.6 times the atmospheric ratio) (33), and ¹⁸O values (5) are substantially different from those expected for uncontaminated mantle-derived magmas. Isotopic ratios of Phlegraean Fields magmas are also in the same range. These isotopic signatures have been shown to be the result of contamination of mantle-derived shoshonitic magmas with continental crust similar in composition to a xenolith found in Phlegraean Fields pyroclastics (7). Crustal contamination would be more effective if the magma sill, consistent with the inferred *P* and *S* velocities, is not a continuous molten body, but if magma is interspersed in a densely fractured rock, with a large ratio of contact surface to melt volume. The variations of Sr isotopic composition observed even during a single eruption (7) indicate the presence of an extremely heterogeneous poorly mixed magma within the feeding system, which suggests a vertically and laterally discontinuous sill-like layer.

References and Notes

1. R. Scandone, L. Giacomelli, P. Gasparini, *J. Volcanol. Geotherm. Res.* **58**, 5 (1993).
2. R. Santacroce, A. Sbrana, A. Bertagnini, L. Civetta, P. Landi, *J. Petrol.* **34**, 383 (1993).

3. R. Cioni *et al.*, *J. Petrol.* **36**, 739 (1995).
4. G. Orsi, M. Piochi, L. Civetta, M. D'Antonio, P. DiGirolamo, *J. Volcanol. Geotherm. Res.* **67**, 291 (1995).
5. R. Ayuso, R. Seal, A. Paone, B. De Vivo, G. Rolandi, *J. Volcanol. Geotherm. Res.* **82**, 53 (1998).
6. S. Black, G. Rolandi, R. MacDonald, B. De Vivo, G. Rolandi, *J. Volcanol. Geotherm. Res.* **82**, 97 (1998).
7. L. Civetta, M. D'Antonio, P. Gasparini, M. Piochi, *Earth Planet. Sci. Lett.*, in press.
8. P. Marianelli, N. Metrich, A. Sbrana, *Bull. Volcanol.* **61**, 48 (1999).
9. P. Fulignati, P. Marianelli, A. Sbrana, *Mineral. Mag.* **64**, 481 (2000).
10. H. Belkin, B. De Vivo, *J. Volcanol. Geotherm. Res.* **58**, 89 (1993).
11. A. Zollo *et al.*, *Science* **274**, 592 (1996).
12. P. Gasparini, TomoVes Working Group, *Eos* **79**, 229 (1998).
13. A. Zollo, R. De Matteis, L. D'Auria, J. Virieux, in *Problems in Geophysics in the New Millennium*, E. Boschi, G. Ekstrom, A. Morelli, Eds. (ING Editrice Compositori, Bologna, Italy, 2000), pp. 125–140.
14. P. Thiery, S. Operto, G. Lambaré, *Geophysics* **64**, 142 (1999).
15. R. De Matteis, D. Latorre, A. Zollo, J. Virieux, *Pure Appl. Geophys.* **157**, 1643 (2000).
16. A. Lomax, A. Zollo, P. Capuano, J. Virieux, *Geophys. J. Int.* **146**, 313 (2001).
17. The synthetic data used in this paper were obtained with a technique based on elastic finite differences computing the full waveform (34).
18. E. Auger, thesis, Université de Nice, Sophia Antipolis (2000).
19. Web fig. 1 is available on Science Online at www.sciencemag.org/cgi/content/full/294/5546/1510/DC1.
20. R. Di Maio *et al.*, *J. Volcanol. Geotherm. Res.* **82**, 219 (1998).
21. W. S. Fyfe, in *Reflection Seismology: The Continental Crust*, M. Baranzagi, L. Brown, Eds. (American Geophysical Union, Washington, DC, 1986), pp. 244–275.
22. R. K. Litac, I. D. Brown, *Eos* **70**, 713 (1989).
23. M. J. Berry, J. A. Mayer, in *The Continental Crust and Its Mineral Deposit*, D. Strangway, Ed. (Geological Association of Canada, Toronto, 1980), pp. 101–106.
24. W. Fluch, G. Mooney, E. F. Ambos, *J. Geophys. Res.* **94**, 16023 (1989).
25. P. Morel a l'huissier, A. Green, C. J. Pike, *J. Geophys. Res.* **92**, 6403 (1987).
26. S. Muller, in *Explosion Seismology in Central Europe*, P. Giese, C. Prodelh, A. Stein, Eds. (Springer Verlag, Berlin, 1977), pp. 289–318.
27. S. Matsumoto, A. Hasegawa, *J. Geophys. Res.* **101**, 3067 (1996).
28. R. Balch, H. Hartsc, A. Sandford, L. Kuo-wan, *Bull. Seismol. Soc. Am.* **87**, 174 (1997).
29. A. F. Stroujkova, P. E. Malin, *Bull. Seismol. Soc. Am.* **90**, 500 (2000).
30. The Elekt Group, *J. Geophys. Res.* **102**, 18289 (1997).
31. N. Christensen, in *Handbook of Physical Properties of Rocks*, vol. 11, R. S. Carmichael, Ed. (CRC Press, Boca Raton, FL, 1982), pp. 1–22.
32. M. P. Ryan, in *Magmatic Systems*, vol. 2, M. P. Ryan, Ed. (Academic Press, London, 1994), pp. 97–138.
33. D. Graham, J. Lupton, P. Allard, C. Kilburn, E. Spera, *J. Volcanol. Geotherm. Res.* **58**, 359 (1993).
34. J. Virieux, *Geophysics* **51**, 889 (1986).
35. To identify *PP* (*PS*) phases, we first compute the exact propagation time for a *PP* (*PS*) reflection upon a 10-km deep interface in a constant velocity medium with $V_p = 6$ km/s and $V_p/V_s = 1.73$. Each trace is then moved along the time axis according to this propagation time. As a result of this "Ray Normal Move Out" processing, *PP* (*PS*) phases should align at 3.3 s (4.5 s).
36. Air gun profiles of the MAREVES experiment were performed by the IFEMER Nadir ship. The project was financially supported by Gruppo Nazionale di Vulcanologia (GNV) and by Ministero dell'Università e della Ricerca Scientifica e Tecnologica. Data processing and interpretation were supported by European Commission Division XII with contract ENV4-CT96-5041.

31 July 2001; accepted 9 October 2001